Nuclear Inst. and Methods in Physics Research B 460 (2019) 193–200

Contents lists available at ScienceDirect

Nuclear Inst. and Methods in Physics Research B

journal homepage: www.elsevier.com/locate/nimb

Ionization probability of sputtered coronene molecules

M. Herder, J. Klein, A. Sevim, A. Wucher*

Fakultät für Physik, Universität Duisburg-Essen, 47048 Duisburg, Germany

ARTICLE INFO

Keywords:
Ion-surface-interaction
Sputtering
SIMS
SNMS
Ionization probability

ABSTRACT

The formation of molecular secondary ions released from a Coronene film under irradiation with a 20-keV C_{60}^+ ion beam is investigated using combined time-of-flight Secondary Ion and Neutral Mass Spectrometry (ToF-SIMS/SNMS). More specifically, the charge state distribution of intact sputtered coronene molecules M is investigated by comparing the yield of molecular ions M^+ with that of their neutral counterparts M^0, with the latter being post-ionized after their ejection from the surface using single photon ionization in a pulsed vacuum-ultraviolet laser beam. A quantitative determination of the molecular ionization probability from such experiments requires precise information regarding the post-ionization efficiency as well as the laser induced photo-fragmentation of the sputtered neutral molecules, which is obtained from the laser intensity dependence of the measured ToF spectra. In order to assess the role of internal excitation encompassed during the sputter ejection process, the results obtained for sputtered molecules are compared with those obtained for thermally evaporated coronene molecules. As a result, we find an ionization probability of sputtered intact coronene molecules of the order of 10^{-3}, which confirms previous data obtained in a similar experiment using a fundamentally different post-ionization scheme.

1. Introduction

The formation of secondary ions during ion sputtering of solid surfaces represents the physical basis of Secondary Ion Mass Spectrometry (SIMS). A key quantity in such experiments is the ionization (or secondary ion formation) probability of a sputtered particle, defined as

$$\alpha_X^{+,-} = \frac{Y_X^{+,-}}{Y_X} \tag{1}$$

where X can stand for a single atom, molecule or cluster emitted from an ion-irradiated sample surface. The quantity $Y_X^{+,-}$ denotes the secondary ion yield, i.e., the average number of secondary ions $X^{+,-}$ which is emitted per projectile impact, while Y_X represents the respective partial sputter yield of all emitted particles X regardless of their charge state. It should be stressed that this definition of $\alpha_X^{+,-}$ does not necessarily imply the emission and ionization processes to be decoupled. While this may in some cases be true, e.g. for single atoms emitted from a clean metallic surface, one could imagine a strong coupling between the ejection and ionization mechanisms in other cases, for instance via a charge related emission process such as Coulomb explosion. Particularly for molecular emission, the fragmentation of a sputtered molecule may also be closely coupled to its charge state, so that the factorization according to Eq. (1) may represent an oversimplification.

In the past, significant effort has been devoted to the investigation of ionization probabilities for atomic species emitted from the irradiated surface. It is common knowledge that $\alpha^{+,-}$ in these cases critically depends on the chemical state of the surface, leading to the so-called SIMS matrix effect. For many samples, the intrinsic ionization probabilities measured at a clean elemental surface are rather small [1], rendering most of the sputtered material electrically neutral, while oxidized surfaces, for instance, yield ionization probabilities which may be enhanced by orders of magnitude [2–4].

Apart from elemental analysis, the ability to deliver molecular information represents one of the outstanding features of the SIMS technique. Particularly for imaging SIMS experiments, where the sample is irradiated with a focused ion beam rastered across the surface, the ionization probability represents one of the key factors limiting the detection sensitivity and, hence, the achievable useful lateral resolution [5–7]. It is therefore of great interest to increase the ionization efficiency of the sputtered material as much as possible, while still preserving its chemical integrity. For molecular species, it has been suggested that the use of cluster ion beams such as Bi_n^+, C_{60}^+ or Ar_n^+ may allow a softer transfer of intact molecules into the gas phase with less sputter induced fragmentation than atomic projectiles [8], and these projectiles are now routinely used in molecular SIMS analysis.

* Corresponding author.
E-mail address: andreas.wucher@uni-due.de (A. Wucher).

https://doi.org/10.1016/j.nimb.2019.05.008
Received 30 October 2018; Received in revised form 22 January 2019; Accepted 3 May 2019
Available online 18 May 2019
0168-583X/

The ionization efficiency of sputtered molecules released by such projectiles, however, is often presumed to be rather low [5], with values down to 10^{-5} being sometimes quoted in the literature [9,10]. Hard experimental evidence for this presumption, on the other hand, is scarce. A quantity that is more readily accessible is the *useful ion yield*, which is defined as the number of detected secondary (molecular) ions divided by the total number of molecule equivalents removed from the sample. Useful yield values for molecular ions under cluster ion impact have in some cases been reported [11,12], showing values of the order of $10^{-6} - 10^{-5}$. Apart from the ionization probability, this quantity includes the probability of a sputtered molecule to survive the emission process intact as well as the instrumental collection efficiency for the emitted secondary ions. Both quantities are unknown, and a proper determination of the ionization probability therefore ultimately requires a mass resolved detection of the emitted neutral and ionized molecules under the same experimental conditions regarding the instrumental collection efficiency. This, in turn, requires the post-ionization of a sputtered neutral molecule with known efficiency, using a post-ionization process which i) is decoupled from the chemical surface state and ii) does not alter the detection efficiency of the resulting ion with respect to the intrinsically emitted secondary ions.

One possible strategy for such experiments is to use laser-induced photoionization in combination with time-of-flight mass spectrometry [13], where the sputtered material is interrogated by a pulsed laser beam and the instrument is operated in such a mode that it cannot distinguish between intrinsic secondary ions and post-ionized photoions. For molecular species, it is important to use a "soft" photoionization scheme that minimizes laser induced fragmentation while at the same time maximizing the post-ionization efficiency. Two different strategies have been proposed for that purpose, namely i) vacuum ultraviolet (VUV) single photon ionization (SPI) [14–19] and ii) infrared (IR) strong field photoionization (SFI) [20–26]. For the particular example of coronene molecules (M) sputtered under irradiation with 20-keV C_{60}^+ projectiles, the SFI technique has been used to determine an ionization probability for M^+ formation of the order of 10^{-3} [27]. In the present work, we repeat this experiment using a fundamentally different SPI photoionization scheme in order to test the robustness of the result against variations of the post-ionization process. The coronene molecule exhibits an ionization energy of 7.21 eV [28] and is therefore ideally suited for VUV single photon ionization using a 157 nm F_2 excimer laser with a photon energy of about 7.9 eV. Using this strategy, we examine the photoionization efficiency as well as the photo-induced fragmentation of sputtered and thermally evaporated coronene molecules as a function of the laser intensity. From the measured saturation behavior, we then determine the photoionization and -fragmentation cross sections and use these data to determine the molecular secondary ion formation probability.

2. Experimental

The experiments were performed using a home-built reflectron time-of-flight (ToF) mass spectrometer described in detail elsewhere [29,30], and therefore only a brief description of the features relevant for this work will be given here. The ToF spectrometer is mounted under 45° with respect to the impinging primary ion beam, and the sample is positioned such that the sputtered particles are collected along the surface normal. The projectile ions are generated by a prototype fullerene ion source (Ionoptika IOG C60) delivering a 20-keV C_{60}^+ ion beam with a current of about 200 pA delivered into a spot size of about 80 μm. The ion beam was operated in a pulsed mode with a pulse duration of about 0.5–5 μs, and the sample was held at ground potential during the ion bombardment. Secondary ions released from the surface could freely expand into the field-free space above the surface and were then swept into the ToF spectrometer using a pulsed extraction field, which was switched on shortly (about 20 ns) after the end of the primary ion pulse. This way, the switching time marked the flight time zero for the detected ions. The reflector voltage (2375 V) was tuned slightly below the target potential (2500 V) in order to ensure that only ions originating from a minimum height of about 0.5 mm above the sample surface could be reflected and detected. In connection with the flight time refocusing properties of the ToF spectrometer, this setting determines a sensitive volume of about 0.5 mm diameter located at about 0.75 mm above the surface and centered around the ion optical axis of the spectrometer, from which ions could be extracted and contribute to the detected sharp flight time peaks [13].

Secondary neutral particles emerging from the bombarded surface were post-ionized using a pulsed F_2-laser (Coherent Excistar XS) operated at a VUV wavelength of 157 nm. The corresponding photon energy ensured that neutral atoms and molecules possessing ionization potentials up to 7.9 eV can be efficiently post-ionized via non resonant single photon absorption. The laser beam was directed parallel to the sample surface at a distance matching the location of the ToF sensitive volume. The beam was focused to a spot of about $0.15 \times 0.4\ mm^2$ (FWHM) in directions perpendicular and parallel to the sample surface, using a 315 mm focal length CaF_2 lens, which at the same time acted as the entrance window to the ultrahigh vacuum chamber housing the experiment. More details regarding the measured beam profile can be found in the supporting information. The laser delivered output pulses of about 4–6 ns duration and up to about 2.5 mJ pulse energy, which was monitored using its internal energy monitor and calibrated using a GenTech power meter. As shown in the supporting information, the maximum energy density in the laser beam focus can then be estimated by multiplying the measured pulse energy by a factor of $800\ cm^{-2}$. The laser beam was guided through an evacuated beam line of about 1 m length and then coupled into the vacuum system via the focusing lens, which had a transmission of about 80%. The laser intensity entering the vacuum chamber was varied by flooding the evacuated beam line with air to different partial pressures, and the resulting energy of the laser pulse actually present in the ionization region was therefore monitored again with the power meter as well as a fast in-vacuum photoelectric detector located behind the sample, the signal of which was also used in order to control the timing of the laser pulse. In order to characterize the focusing conditions of the laser beam, a 50 μm diameter aperture was mounted at the sample holder and scanned across the beam in directions perpendicular and parallel to the sample surface.

During most of the experiments, the laser pulse was fired simultaneously with the ion extraction pulse. This way, the instrument cannot distinguish between intrinsic secondary ions and post-ionized neutral particles of the same species, thereby detecting both entities under otherwise the same experimental conditions regarding instrument collection efficiency, transmission and detection efficiency. In order to distinguish between secondary ions and post-ionized neutrals, spectra were therefore taken with (SNMS) and without (SIMS) firing the laser beam, and the data corresponding to the secondary neutral particles alone were derived by subtracting both spectra.

Secondary ions and post-ionized neutral particles were detected using a Chevron stack of two microchannel plates (MCP) equipped with a grounded entrance grid. Before the MCP stack, a set of blanking plates was mounted to enable the blocking of selected ions from reaching the detector. The MCP output current was measured on a collector plate and digitized using a fast transient digitizer board (Signatec PX 1500). The 8 bit digitizer delivers byte values between 0 and 255, which will in the following be referred to as "cts". Note that the unit of 1 ct defined this way does *not* correspond to the registration of one ion, but rather symbolizes a detected MCP output signal of about 2.0 mV height, which is generated at the 50 Ω input impedance of the transient digitizer and therefore corresponds to an MCP output current of 40 μA. The conversion of this signal into the number of actually detected ions depends on the MCP gain voltage setting. For that purpose, the flight time peak corresponding to a particular mass must be integrated, and the resulting peak integral must be divided by the average peak integral induced by a single ion impact of the same mass. In most cases, the data were

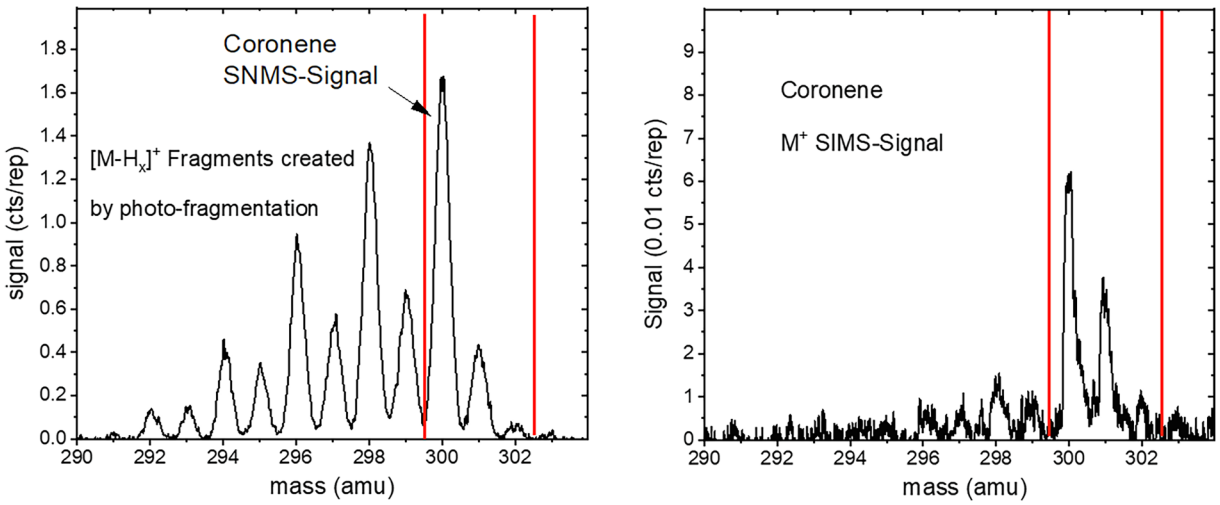

Fig. 1. Mass spectra of post-ionized neutrals (left panel, SNMS) and secondary ions (right panel, SIMS) measured under irradiation of a coronene with 20-keV C_{60}^+ ions. The spectra were averaged over 2000 (SNMS) and 20,000 (SIMS) primary ion pulses ("reps"). The SNMS data were measured at a post-ionization laser pulse energy of about 0.4 mJ.

summed over many acquired primary ion pulses ("reps"). To allow an easy comparison, the measured signal will in the following be normalized to the number of reps and displayed in units of "cts/rep".

The coronene samples were produced by evaporating a molecular film onto a silicon substrate. 10 mm × 10 mm silicon shards were ultrasonically cleaned in acetone and introduced into an ultrahigh vacuum chamber containing a tungsten crucible filled with coronene powder (Aldrich C84801), which was heated by electron impact. During the film deposition, the substrate was held at about 130 K, and the evaporation rate was monitored using a quartz crystal microbalance. Coronene films were deposited to thicknesses between 50 and 150 nm, which were measured ex-situ using an atomic force microscope (KLA Tencor Nanopics 2100). The samples were covered by a molybdenum mask with a central aperture of about 1 mm. This way, it was possible to directly compare the laser intensity dependence of the coronene signals with that measured for Mo atoms sputtered from the molybdenum mask under otherwise the same instrumental conditions [13]. Due to the large difference in signal levels, SIMS and SNMS spectra were measured by averaging over different number of primary ion pulses. During spectrum acquisition, the primary ion beam was rastered across a surface area of 0.3 mm^2. SNMS spectra were typically collected with a total ion fluence of about 10^9 ions/cm^2, while the corresponding SIMS spectrum was typically collected with a total ion fluence of the order of 10^{10} ions/cm^2. A typical experiment consisted of first taking a SIMS spectrum, then taking a series of SNMS spectra at different laser intensities, followed by another SIMS spectrum in order to check for possible damage accumulation effects. The total ion fluence applied in the course of such an experiment was below 10^{11} ions/cm^2, so that the entire experiment was performed in static mode. No significant pre-bombardment of the coronene film was performed in order to preserve the molecular film and prevent ion induced damage accumulation at the surface. In some experiments, coronene molecules were thermally evaporated from the sample surface. For that purpose, the sample holder was heated to approximately 80 °C by blowing heated nitrogen gas through the stage cooling system.

3. Results and discussion

The mass spectrometric signal measured for a secondary ion X^+ or X^- and its neutral counterpart X^0 can be formally described by

$$S(X^{+,-}) = I_p \cdot Y_X \cdot \eta \cdot \alpha_X^{+,-} \quad \text{and}$$
$$S(X^0) = I_p \cdot Y_X \cdot \eta \cdot (1 - \alpha_X^+ - \alpha_X^-) \cdot \alpha_X^0 \qquad (2)$$

where I_p denotes the projectile current, Y_X is the partial sputter yield of species X (regardless of its charge state) and α_X^0 stands for the post-ionization efficiency of the sputtered neutrals. The quantity $\alpha_X^{+,-}$ denotes the probability for a sputtered particle X to leave the surface in a charged state as defined in Eq. (1), which can in principle be determined from a quantitative comparison of measured secondary ion and neutral signals provided the post-ionization efficiency α_X^0 is known. The detection efficiency η describes the fraction of emitted species (secondary ions or post-ionized neutrals) which is effectively sampled by the mass spectrometer. It is determined by the accepted emission velocity and angle window of the ToF spectrometer, which are identical for secondary ions and neutrals if the post-ionization laser illuminates the entire sensitive volume of the mass spectrometer [13]. In this context, it is important to note that our experiment is sensitive to the *number density* of sputtered particles within the sensitive volume rather than their *flux*. Therefore, if ions and neutrals were emitted with different velocity distributions, this would lead to a correction factor, which has been found to be of the order of a factor 2 [30] and will be disregarded here since we are mainly interested in the order of magnitude rather than the exact value of the ionization probability.

3.1. Mass spectra

Mass spectra of post-ionized neutral particles and secondary ions measured on a coronene film irradiated by 20-keV C_{60}^+ ions are shown in Fig. 1. For better visibility, only the relevant mass range around the peaks of the intact parent coronene molecule is shown.

It is seen that the SIMS spectrum (right hand panel of Fig. 1) consists mainly of the molecular secondary ion M^+ with M denoting the parent $C_{24}H_{12}$ coronene molecule at *m/z* 300. The second peak at *m/z* 301 arises in part from the ^{13}C isotope satellite of M^+, which, however, should only amount to 27% of the *m/z* 300 signal. The remaining signal at *m/z* 301 must therefore arise from the protonated $[M + H]^+$ molecule, the signal of which amounts to about 35% of that of M^+. This observation of two competing secondary ion formation channels is consistent with previous SIMS data [27] and appears to be typical for the coronene molecule.

Comparing the SIMS spectrum with the SNMS spectrum depicted in the left hand panel of Fig. 1, one immediately finds that the secondary ions represent only a minor fraction of the sputtered molecules. The spectrum of post-ionized neutral particles contains the intact coronene molecule along with a series of fragments at lower masses. The *m/z* 301/300 peak ratio now exactly reflects the ^{13}C satellite value, so that

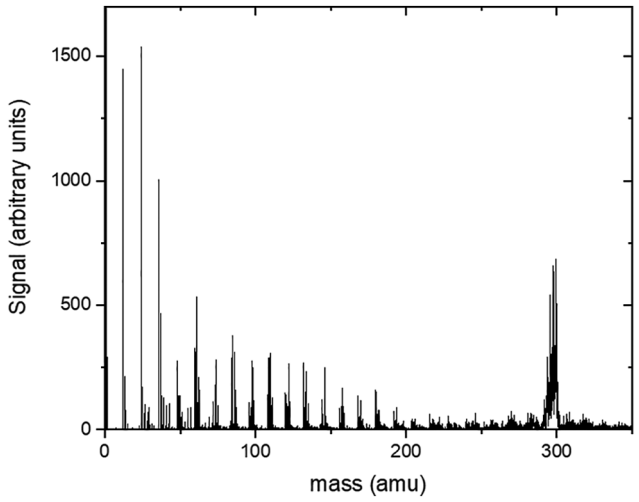

Fig. 2. Mass spectrum of post-ionized neutral particles measured under irradiation of a coronene film with 20-keV C_{60}^+ ions. The data were measured at a post-ionization laser pulse energy of about 0.6 mJ.

the signal detected within the red bars exclusively represents the intact coronene molecule which has been post-ionized without photo-fragmentation. The series of peaks towards smaller masses correspond to the molecule losing a sequential number of hydrogen atoms. They reveal an odd-even alternation, which shows that the loss of a H_2 molecule is favored against that of a single H atom.

As seen from the full spectrum shown in Fig. 2, there is also a series of smaller fragments visible in the SNMS spectrum, which are spaced by 12 amu and correspond to C_nH_m clusters. In principle, these signals may arise either from post-ionization of neutral fragments generated in the course of the sputtering process or from photofragmentation of sputtered intact molecules. It is not easy to distinguish between these possibilities. Moreover, low mass fragmentation signals may be amplified by multiple fragmentation chain reactions, and further low mass signals may also arise from photoionization of residual gas particles. Depending on the laser intensity, the low mass signals can become quite large and lead to detector saturation for molecular signals measured at larger masses. We therefore chose to routinely block all ions below *m/z* 60 from reaching the detector by pulsing the blanking plates in front of the MCP. In order to be comparable, SIMS spectra were then also recorded in this "peak blanking" mode.

3.2. Post-ionization efficiency

A crucial point regarding the quantitative comparison of secondary ion and neutral signals is the post-ionization efficiency, which is governed by the overlap between the laser beam profile, the number density distribution of sputtered neutral particles above the surface and the sensitive volume of the mass spectrometer. Formally, the post-ionization efficiency entering Eq. (2) can be described by

$$\alpha_X^0 = \int_V n_X(\vec{r}) \cdot p_i(\vec{r}) \cdot T(\vec{r}) d^3r, \tag{3}$$

where $n_X(\vec{r})$ denotes the number density of neutral particles, $T(\vec{r})$ is the transmission and detection probability for a photo-ion created at position $\vec{r}$ and the integral has to be taken over the sensitive volume of the mass spectrometer. The photoionization probability p_i depends on the laser intensity and will therefore be position dependent according to the laser beam profile. For the single photon ionization process used here, it is expected to depend on the laser intensity I_L as

$$p_i(I_L) \propto [1 - \exp(-I_L/I_{sat})] \tag{4}$$

where I_{sat} is a saturation intensity depending on the photoabsorption cross section. As long as $I_L \ll I_{sat}$, Eq. (4) describes a linear dependence and the overall post-ionization efficiency described by Eq. (3) will depend linearly on I_L regardless of the shape of the laser beam intensity profile. As soon as I_L reaches I_{sat} anywhere in the sensitive volume, deviations from the linear dependence will occur, until the ionization probability eventually reaches a plateau in the limit of large laser intensities. Unfortunately, the exact shape of the saturation curve is complicated by the fact that both the target density n_X and the detection probability T generally depend on the position within the sensitive volume. Only in the case where the laser beam is defocused such as to illuminate the entire sensitive volume with essentially the same intensity, the photoionization probability p_i can be extracted from the integral in Eq. (3). Under these conditions, the laser intensity dependence of the post-ionization signal measured for an atomic species follows the prediction of Eq. (4) (see [13] and references therein).

For molecules, additional complications arise from the possibility of laser induced photofragmentation. On one hand, fragmentation can occur as a consequence of a single photon absorption and compete with the intact ionization channel discussed above. In that case, the laser intensity dependence of the measured molecular signal will be the same as without fragmentation, with the only difference being that the prediction of Eq. (4) must be multiplied by a constant factor, yielding the measured signal as

$$S(I_L) = S_{sat} \frac{\sigma_i}{\sigma_i + \sigma_f^{(0)}} [1 - \exp\{-(\sigma_i + \sigma_f^{(0)}) I_L\}] \tag{5}$$

Here, the quantities σ_i and $\sigma_f^{(0)}$ denote the single photon ionization and fragmentation cross sections of the neutral molecule, I_L is the laser intensity (in photons/cm^2) and S_{sat} is the hypothetical signal that would be measured if all molecules present in the interaction volume were ionized without fragmentation. For the case investigated here, the available photon energy only permits *neutral* fragmentation, where the coronene molecule absorbs a single photon and breaks up into neutral fragments which are not detectable in the mass spectrum. In order to arrive at a fragment *ion*, the photon energy must be sufficiently large to overcome the sum of dissociation and ionization energies, which is not fulfilled in the present case. On the other hand, *multiphoton* fragmentation can occur, where a single-photon-ionized molecule absorbs more photons and fragments, leading to a detectable decay of the measured signal at high laser intensity. In a simple linear rate equation model, the measured signal should then follow

$$S(I_L) = S_{sat} \frac{\sigma_i}{\sigma_i + \sigma_f^{(0)} - \sigma_f^{(i)}} [1 - \exp\{-(\sigma_i + \sigma_f^{(0)} - \sigma_f^{(i)}) I_L\}] \times \exp(-\sigma_f^{(i)} I_L) \tag{6}$$

where $\sigma_f^{(i)}$ now denotes the fragmentation cross section of the ionized molecule. For the special case where $\sigma_f^{(i)} \simeq \sigma_f^{(0)} \simeq \sigma_f$, Eq. (6) reduces to

$$S(I_L) = S_{sat} [1 - \exp\{-(\sigma_i) I_L\}] \times \exp(-\sigma_f I_L) \tag{7}$$

The laser intensity dependence predicted by Eq. (7) is illustrated in Fig. 3. In view of the experimental data shown below, the result is plotted for the special case where $\sigma_f \simeq \sigma_i$. As a general feature, the measured signal will go through a maximum at the saturation intensity $I_{sat} \simeq \sigma_i^{-1}$, where the signal level only shows a fraction of its hypothetical saturation value S_{sat}. In the limit of low laser intensity, the signal exhibits the same linear slope as in the fragmentation-free case, while it will go to zero in the limit of high laser intensity.

The experimentally measured laser intensity dependence of the post-ionization signal detected for sputtered coronene molecules is shown in Fig. 4 (black dots). It is important to note that only the true M^+ molecule signal obtained by integrating the peak at *m/z* 300 is plotted here, since it was discovered that the $[M-H_x]^+$ fragment ion signals shown in Fig. 1 exhibit a different laser intensity dependence (see below). It is seen that the data resemble the functional form depicted in Fig. 3, with the measured molecular ion signal going through a maximum at a laser pulse energy of about 0.25 mJ and decreasing again

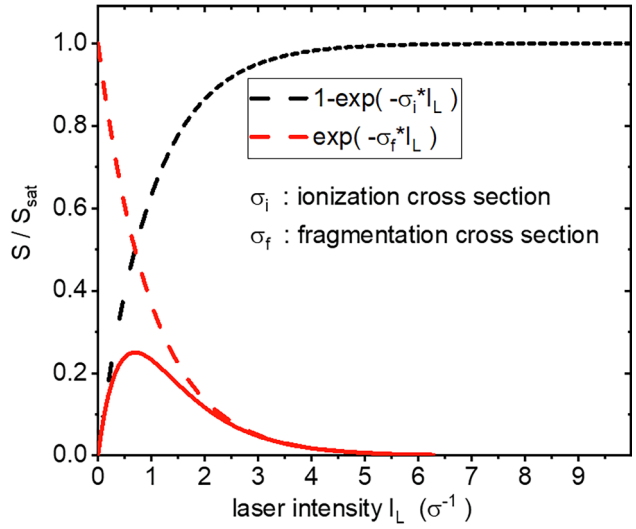

Fig. 3. Laser intensity dependence of a molecular ion signal as predicted by Eq. (7) in the text. Solid line: full calculation; dashed lines: ionization and fragmentation terms plotted separately. The calculation was performed for the special case where$\sigma_f = \sigma_i$

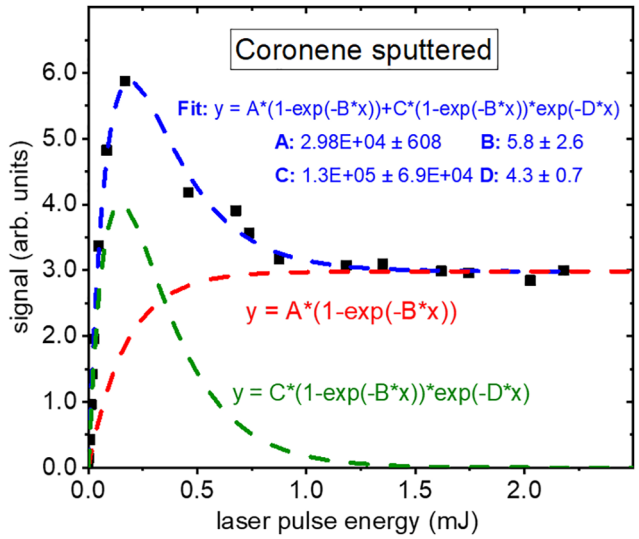

Fig. 4. Laser intensity dependence of the signal measured for post-ionized sputtered neutral coronene molecules. Black dots: experimental data; dashed lines: least square fits of the indicated functions.

at higher laser intensities. There is, however, a significant difference related to the asymptotic behavior of the signal at high laser intensity. In contrast to the prediction of Eq. (7), the measured signal does not go to zero in this limit, but approaches a constant plateau value. This behavior indicates that the measured signal must arise from two different contributions, with one part of the sputtered molecules undergoing multiphoton fragmentation and another part being stable in the accessible laser intensity range. In fact, the measured signal variation can be fitted to a functional dependence characterized by the sum of two terms, both described by Eq. (7) using the same values of the ionization cross section σ_i but different fragmentation behavior. The first term features a fragmentation cross section σ_f which is comparable to the ionization cross section, thereby leading to the observed signal maximum as illustrated in Fig. 3. From the position of the maximum at a laser pulse energy of about 0.25 mJ, it is evident that this signal contribution, which is displayed as the green dashed curve in Fig. 4, must decay to essentially zero at laser pulse energies above 1.5 mJ. The second contribution, indicated by the red dashed line in Fig. 4, reaches a plateau in this laser intensity range. It must therefore be characterized by a fragmentation cross section which is significantly smaller than the ionization cross section, leading to a negligible signal decay in the laser intensity range accessible here. This contribution was therefore fitted by setting the value of σ_f to zero. The blue solid line then represents the sum of both contributions, which is seen to represent a good fit to the measured data.

From the above discussion, it appears that the flux of sputtered neutral coronene molecules must contain two different species, with one molecule being significantly more susceptible to multiphoton fragmentation than the other. The question of course arises regarding the difference between both species. In both cases, we are obviously detecting sputtered neutral parent molecules which survive the sputter ejection process intact. On the other hand, it is well known that the collision-dominated sputtering event may impart significant amounts of internal energy to an ejected molecule, so that the different photofragmentation behavior may in principle arise from differences in the internal excitation state of the ejected molecules. In fact, it appears feasible that the photoabsorption cross section of an internally excited molecule may significantly differ from that of a ground state molecule [31]. In order to test this hypothesis, we have repeated the post-ionization experiment for neutral coronene molecules that were thermally evaporated from the sample surface and analyzed under otherwise the same instrumental conditions. The philosophy behind this experiment is that these molecules contain less internal energy and may therefore represent a model case for the non-fragmenting part of the sputtered molecules.

Fig. 5 shows the resulting laser intensity dependence of the molecular ion signal measured under these conditions. It is immediately evident that the fragmentation behavior is completely different from that depicted in Fig. 4. In fact, the signal variation can be approximated by setting the fragmentation cross section in Eq. (7) to zero. The corresponding least square fits to the two data sets shown in Fig. 5 are indicated by the dashed lines. In particular, it is of note that the fitting parameter $B \sim 4.1 \pm 0.3\,\mathrm{mJ}^{-1}$ representing the photoionization cross section agrees within the error bars with that determined for the sputtered molecules ($B \sim 5.8 \pm 2.6\,\mathrm{mJ}^{-1}$). From these results, we conclude that the interpretation of two different contributions within the flux of sputtered coronene molecules is probably correct. Inspection of the fitting parameters A and C depicted in Fig. 4 reveals that about 19% of the sputtered molecules are ejected close to the ground state,

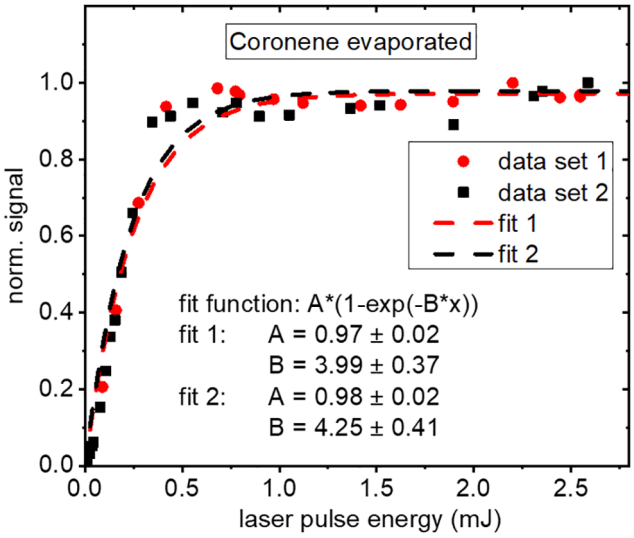

Fig. 5. Laser intensity dependence of the signal measured for post-ionized neutral coronene molecules that were thermally desorbed from the coronene film. Black and red dots: experimental data; dashed lines: least square fits of the indicated function.

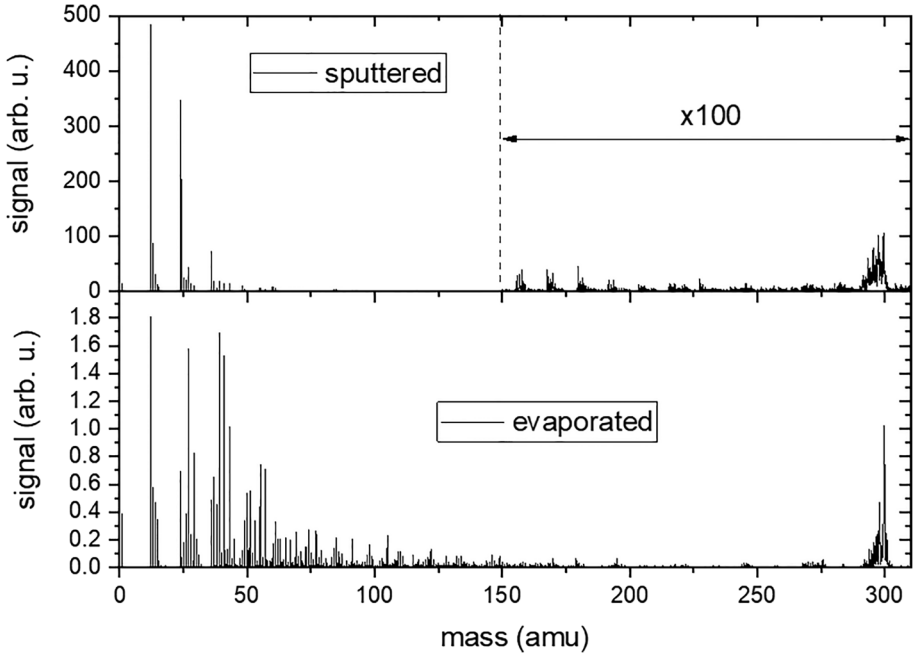

Fig. 6. Mass spectrum of post-ionized evaporated coronene measured at the highest available laser intensity of 2.5 mJ/pulse.

while 81% leave the surface in an internally excited state that makes them susceptible to multiphoton absorption and fragmentation.

Of course, the "ideal" saturation behavior measured for the molecular ion signal as observed in Fig. 5 does not mean that there is no laser induced fragmentation. This becomes immediately evident by looking at the mass spectrum measured for evaporated coronene molecules, which is shown for the largest available laser intensity in Fig. 6. Apart from the molecular ion signal, the spectrum shows pronounced signals of $[M-H_x]^+$ fragments as well as other, less prominent characteristic fragments such as $[M-C_2]^+$ along with a series of unspecific low mass peaks spaced by 12 amu. The latter can be traced to $[C_nH_m]^+$ ions which probably arise from multiple fragmentation reactions. The strong $[M-H_x]^+$ signals reflect the fact that the loss of a hydrogen atom constitutes the energetically favored evaporative cooling mechanism of an excited coronene molecule with the lowest dissociation energy of 4.5 eV [32]. In order to shed more light on the origin of the fragment ion signals, Fig. 7 shows the laser intensity dependence measured for the molecule-specific $[M-H_x]^+$ ions summed over the m/z 292–299 range along with an unspecific C_3^+ fragment at m/z 36. For comparison, the data measured for intact coronene molecules have been included in the figure. It is seen that the fragment signals exhibit a nonlinear increase at low laser intensities, which is in pronounced contrast to the linear dependence of the molecular ion signal and reveals that the fragment ions must be produced via multiphoton processes. Since the molecular ion signal does not decrease at high laser intensity, it is evident that the increasing fragment ion signals must arise from photoionization of neutral species, which may either be directly emitted from the sample surface or produced via photofragmentation of the desorbed intact molecules. The first possibility appears unlikely, since investigations of coronene clusters have revealed that the temperature needed for thermal fragmentation of a coronene molecule is significantly larger than that for its intact desorption [32]. The same study concludes that an internal energy of at least 12 eV is necessary for a coronene molecule to evaporate a hydrogen atom on a time scale of 10 μs, thereby effectively ruling out single photon induced neutral fragmentation and explaining the multiphoton nature of the observed fragment ion signals. Particularly the small, unspecific fragment ions such as C_2^+, C_3^+ etc. exhibit power law slopes

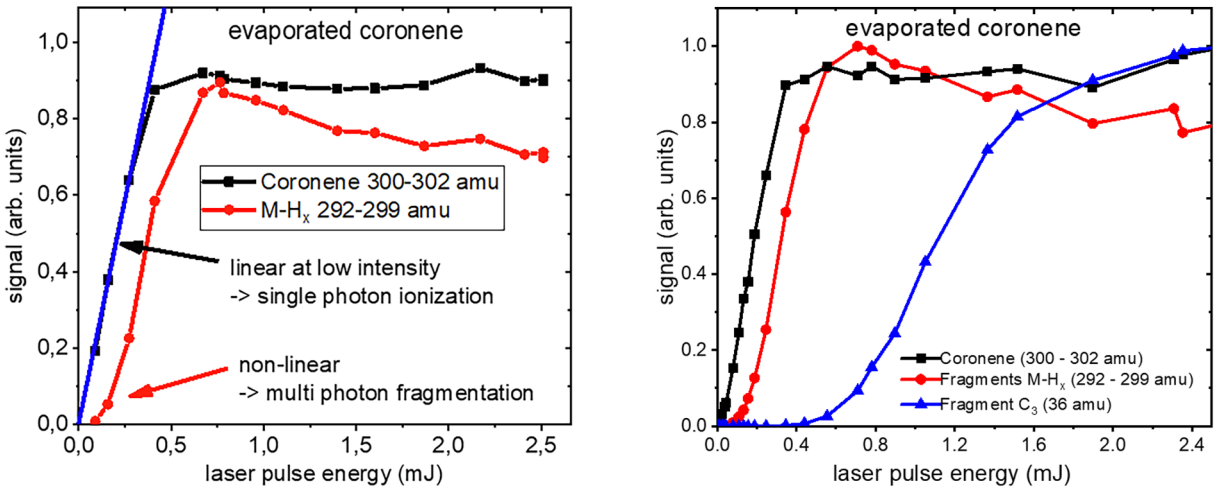

Fig. 7. Laser intensity dependence of selected fragment signals measured during evaporation of coronene molecules.

Table 1
Secondary ion signal and (hypothetical) saturated post-ionization signal of sputtered coronene molecules integrated over the mass range delimited by the red bars in Fig. 1. Third row: secondary ion formation probability α_M^+ determined from the SIMS/SNMS signal ratio.

	Data set #1	Data set #2	Data set #3
SIMS	7.75	0.38	5.50
SNMS (S_{sat})	810	54.3	515
SIMS/SNMS	9.5×10^{-3}	7.0×10^{-3}	1.1×10^{-2}
α^+ (frag. corrected)	3.2×10^{-3}	2.3×10^{-3}	3.6×10^{-3}

which indicate that 5 and more photons are needed for their generation, indicating that these signals probably arise from multiple photofragmentation chains. At laser energies below 0.25 mJ/pulse, all fragmentation signals are small, leading to a rather clean molecular ion spectrum. In the regime of high laser intensity, the $[M-H_x]^+$ fragment signals appear to decrease again, thereby illustrating the occurrence of secondary fragmentation reactions induced by further photon absorption.

As a consequence of these discussions, we conclude that the (hypothetical) saturation signal S_{sat} determined from the fits indicated in Fig. 4 and Fig. 5 represents a lower limit of the true density of neutral molecules that are present in the interaction volume. In order to arrive at an estimate of the possible influence of photofragmentation, we relate the signal measured for evaporated intact coronene molecules (m/z 300–302) to that of all fragments detected in the mass range between m/z 150 and m/z 299. The restriction to half of the molecule mass ensures that each fragmentation reaction is counted only once. The resulting signal ratio measured at the highest laser intensity, where the photoionization of the most prominent fragments appears to be saturated, is 0.57, indicating that at least 36% of the evaporated coronene molecules survive the photoionization process intact. Assuming the same fraction for the sputtered molecules as well, the value of S_{sat} determined above must be multiplied by roughly a factor 3.

3.3. Ionization probability

If the effective post-ionization efficiency is known, the secondary ion formation probability α^+ of a sputtered coronene molecule can be directly determined from the quantitative comparison of post-ionization and secondary ion signals. From the discussion in the preceding subsection, we conclude that the sum of the fitting parameters A and C constitutes the saturation signal S_{sat} of sputtered neutral molecules present in the sensitive volume. In order to correct for photofragmentation as explained above, this signal must further be multiplied by a factor 3. The resulting (hypothetical) saturation signal of neutral molecules can now be compared to that measured for the secondary ions. i.e., without firing the post-ionization laser, under otherwise identical experimental conditions. Integrating the corresponding peaks in the mass range delimited by the red bars in Fig. 1, one finds the molecular SIMS signals which are listed in Table 1 along with the corresponding (hypothetical) saturated SNMS signals. Since the SNMS spectra contain the SIMS signals as well, the ionization probability is then simply determined by the SIMS/SNMS signal ratio. The resulting values extracted from three different data sets are also displayed in Table 1. Applying the photofragmentation correction discussed above, one obtains the secondary ion formation probability α_M^+ depicted in the bottom row.

The available data indicate an average secondary ion formation probability of about 3×10^{-3}. It should be noted that – for the particular case of the coronene molecules investigated here - this quantity includes the formation of M^+ molecular ions as well as $[M+H]^+$ protonated molecules. In principle, the removal of an electron from the otherwise chemically unaltered molecule requires some form of transient electronic excitation in the course of the sputtering process. From the discussion of the SIMS spectra in Fig. 1, we find that the probability for such a "physical" ionization mechanism leading to M^+ formation is about $\alpha_{phys}^+ = 2.2 \times 10^{-3}$, while the "chemical" ionization leading to $[M+H]^+$ formation occurs with a probability of $\alpha_{chem}^+ = 8 \times 10^{-4}$. The value of α_{phys}^+ can be compared to corresponding data obtained from a similar experiment using a different post-ionization scheme. Utilizing strong field photoionization of neutral coronene molecules sputtered from a similar sample as used here under irradiation with 40-keV C_{60}^+ ions and applying the same photofragmentation correction as used here, Popczun et al. [27] determined the M^+ formation probability as 2.5×10^{-3}. In view of the largely different photoionization methods employed in both experiments, the agreement with the α_{phys}^+ value determined here is remarkable. It shows that at least the order of magnitude of the secondary ion formation probability measured for sputtered organic molecules using the laser post-ionization technique is reliable.

4. Conclusions

The experiments performed here again corroborate the notion that the ion fraction of organic molecules sputtered from a bulk molecular film under irradiation with cluster ion beams is small. Here, corresponding data were obtained for intact coronene molecules ejected from a ~10 nm-thick coronene film irradiated with 20 or 40 keV C_{60}^+ projectile ions. The coronene molecule is a rare example where both the "physical" ionization mechanism leading to the formation of molecular ions M^+ and the "chemical" protonation mechanism leading to $[M+H]^+$ formation are both operational with comparable efficiency. From the comparison of the respective secondary ion signals with those measured via single photon post-ionization of the sputtered neutral molecules, we find physical and chemical ionization probabilities of the order of 10^{-3}, with the M^+ formation channel dominating over protonation by a roughly a factor three. Even though there is some remaining ambiguity related to possible photofragmentation of the sputtered neutral molecules, the data indicate that there is headroom of about two orders of magnitude for improvement of the SIMS ionization probability. Data collected recently using strong field laser post-ionization indicate that this headroom might be even larger for other cluster ion beams such as Ar_n [33]. Studies of the kind performed here may therefore motivate further efforts to improve the detection sensitivity of molecular SIMS experiments via methods to enhance the ionization efficiency of the sputtered molecules.

Acknowledgement

The authors acknowledge financial support from the German Ministry of Science (BMBF) in the framework of the Verbundprojekt 05K2016 "Ion Induced Materials Characterization and Modification" and the Deutsche Forschungsgemeinschaft (DFG, German Science Foundation) Projektnummer 278162697 - SFB 1242.

Appendix A. Supplementary data

Supplementary data to this article can be found online at https://doi.org/10.1016/j.nimb.2019.05.008.

References

[1] A. Wucher, H. Oechsner, Absolute ionization probabilities in secondary ion emission from clean metal surfaces, in: j. Romig, W.F. Chambers (Eds.) Proc. of 21st Annual Conference of the Microbeam Analysis Society 1986, San Francisco Press, 1986.
[2] J. München, D. Lipinsky, H.F. Arlinghaus, Signals of secondary ions and resonantly and nonresonantly ionized neutrals sputtered from binary alloys as a function of oxygen exposure, Surf. Interf. Anal. 45 (2013) 117–121.
[3] A. Benninghoven, Developments in secondary ion mass spectroscopy and applications to surface studies, Surf. Sci. 53 (1975) 596–625.
[4] A. Wucher, H. Oechsner, Emission energy dependence of ionization probabilities in

secondary ion emission from oxygen covered Ta, Nb and Cu surfaces, Surf. Sci. 199 (1988) 567–578.
[5] J.C. Vickerman, N. Winograd, SIMS-A precursor and partner to contemporary mass spectrometry, Int. J. Mass Spectrom. 377 (2015) 568–579.
[6] J. Vickerman, N. Winograd, Cluster TOF-SIMS imaging and the characterization of biological materials, in: Cluster Secondary Ion Mass Spectrometry, John Wiley & Sons, Inc., 2013, pp. 269-312.
[7] J.S. Fletcher, N.P. Lockyer, J.C. Vickerman, Developments in Molecular Sims Depth Profiling and 3D Imaging of Biological Systems Using Polyatomic Primary Ions, Mass Spectrometry Rev. 30 (2011) 142–174.
[8] N. Winograd, The magic of cluster SIMS, Anal. Chem. 77 (2005) 142A–149A.
[9] J.S. Fletcher, J.C. Vickerman, A new SIMS paradigm for 2D and 3D molecular imaging of bio-systems, Anal. Bioanal. Chem. 396 (2010) 85–104.
[10] S. Sheraz, A. Barber, I.B. Razo, J.S. Fletcher, N.P. Lockyer, J.C. Vickerman, Prospect of increasing secondary ion yields in ToF-SIMS using water cluster primary ion beams, Surf. Interf. Anal. 46 (2014) 51–53.
[11] J. Zhang, K. Franzreb, S.A. Aksyonov, P. Williams, Mass Spectra and Yields of Intact Charged Biomolecules Ejected by Massive Cluster Impact for Bioimaging in a Time-of-Flight Secondary Ion Microscope, Anal. Chem. 87 (2015) 10779–10784.
[12] A. Wucher, Molecular ionization probability in cluster-SIMS, Journal of Vacuum Science & Technology B, Nanotechnology and Microelectronics: Materials, Processing, Measurement, and Phenomena 36 (2018) 03F123.
[13] A. Wucher, Laser postionization - fundamentals, in: J.C. Vickerman, D. Briggs (Eds.), TOF-SIMS: Materials analysis by mass spectrometry, IM Publications and SurfaceSpectra, 2013, pp. 217–246.
[14] J.B. Pallix, U. Schuehle, C.H. Becker, L. Huestis, Advantages of Single-Photon Ionization over Multiphoton Ionization for Mass Spectrometric Surface Analysis of Bulk Organic Polymers, Anal. Chem. 61 (1989) 805–811.
[15] N.P. Lockyer, J.C. Vickerman, Single Photon Ionisation Mass Spectrometry using Laser-generated Vacuum Ultraviolet Photons, Laser Chem. 17 (1997) 139–159.
[16] M. Wahl, A. Wucher, VUV photoionization of sputtered neutral silver clusters, Nucl. Instrum. Methods B 94 (1994) 36–46.
[17] L.K. Takahashi, J. Zhou, K.R. Wilson, S.R. Leone, M. Ahmed, Imaging with Mass Spectrometry: A Secondary Ion and VUV-Photoionization Study of Ion-Sputtered Atoms and Clusters from GaAs and Au, J. Phys. Chem. A 113 (2009) 4035–4044.
[18] I.V. Veryovkin, W.F. Calaway, J.F. Moore, M.J. Pellin, J.W. Lewellen, Y.L. Li, S.V. Milton, B.V. King, M. Petravic, A new horizon in secondary neutral mass spectrometry: post-ionization using a VUV free electron laser, Appl. Surf. Sci. 231–2 (2004) 962–966.
[19] L. Hanley, P.D. Edirisinghe, W.F. Calaway, I.V. Veryovkin, M.J. Pellin, J.F. Moore, 7.87 eV Postionization of Peptides Containing Tryptophan or Derivatized with Fluorescein, Appl. Surf. Sci. 252 (2006) 6723–6726.
[20] R.J. Levis, M.J. Dewitt, Photoexcitation, ionization, and dissociation of molecules using intense near-infrared radiation of femtosecond duration, J. Phys. Chem. A 103 (1999) 6493–6507.
[21] M.J. Dewitt, R.J. Levis, Concerning the ionization of large polyatomic molecules with intense ultrafast lasers, J. Chem. Phys. 110 (1999) 11368–11375.
[22] A.N. Markevitch, S.M. Smith, D.A. Romanov, H.B. Schlegel, M.Y. Ivanov, R.J. Levis, Nonadiabatic dynamics of polyatomic molecules and ions in strong laser fields, Phys. Rev. A 68 (2003) 011402–011406.
[23] D. Willingham, D.A. Brenes, N. Winograd, A. Wucher, Investigating the fundamentals of molecular depth profiling using strong-field photoionization of sputtered neutrals, Surf. Interf. Anal. 43 (2011) 45–48.
[24] A. Kucher, N. Winograd, Strong-field ionization of C-60 sputtered neutral molecules using 10(15) W/cm(2) of fs IR radiation, Surf. Interf. Anal. 45 (2013) 510–512.
[25] A. Longobardo, A.N. Macpherson, J.C. Vickerman, N.P. Lockyer, New prospects for molecular post-ionisation using femtosecond IR lasers, Surf. Interf. Anal. 45 (2013) 525–528.
[26] A. Kucher, L.M. Jackson, J.O. Lerach, A.N. Bloom, N.J. Popczun, A. Wucher, N. Winograd, Near infrared (NIR) strong field ionization and imaging of C_{60}-sputtered molecules: overcoming matrix effects and improving sensitivity, Anal. Chem. 86 (2014) 8613–8620.
[27] N.J. Popczun, L. Breuer, A. Wucher, N. Winograd, On the SIMS ionization probability of organic molecules, J. Am. Soc. Mass Spectr. 28 (2017) 1182–1191.
[28] D. Schröder, J. Loos, H. Schwarz, R. Thissen, D.V. Preda, L.T. Scott, D. Caraiman, M.V. Frach, D.K. Böhme, Single and Double Ionization of Corannulene and Coronene, Helvetica Chimica Acta 84 (2001) 1625–1634.
[29] R.M. Braun, P. Blenkinsopp, S.J. Mullock, C. Corlett, K.F. Willey, J.C. Vickerman, N. Winograd, Performance characteristics of a chemical imaging time-of-flight mass spectrometer, Rapid Commun. Mass Spectr. 12 (1998) 1246–1252.
[30] P. Mazarov, A. Samartsev, A. Wucher, Determination of energy dependent ionization probabilities of sputtered particles, Appl. Surf. Sci. 252 (2006) 6452–6455.
[31] H. Tai, M.R. Flannery, Photoionization of vibrationally excited molecular hydrogen, Phys. Rev. A 16 (1977) 1124–1135.
[32] M. Schmidt, A. Masson, C. Bréchignac, Coronene cluster experiments: stability and thermodynamics, Int. J. Mass Spectrom. 252 (2006) 173–179.
[33] L. Breuer, H. Tian, A. Wucher, N. Winograd, Molecular SIMS ionization probability studied with laser post-ionization: influence of the projectile cluster, J. Phys. Chem. C (2019).